ORIGINAL ARTICLE

Automatic control of UAVs: new adaptive rules and type-3 fuzzy stabilizer

Jinya Cai[1] · Haiping Zhang[2] · Amith Khadakar[3] · Ardashir Mohammadzadeh[4,5] · Chunwei Zhang[4]

Abstract

Unmanned Aerial Vehicles (UAVs) have become important in an extensive range of fields such as surveillance, environmental monitoring, agriculture, infrastructure inspection, commercial applications, and many others. Ensuring stable flight and precise control of UAVs, especially in adverse weather conditions or turbulent environments, presents significant challenges. Developing control systems that can adapt to these environmental factors while ensuring safe and reliable operation is a main motivation. Considering the challenges, first, an adaptive model is identified using the input/output data sets. New adaptation laws are obtained for dynamic parameters. Then, a Type-3 (T3) Fuzzy Logic System (FLS) is used to compensate for the error of dynamic identification. T3-FLS is tuned by a sliding mode control (SMC) strategy. The robustness is analyzed considering the adaptation error using the SMC approach. The main idea is that the basic dynamics of UAVs are taken into account, and adaptation laws are designed to enhance the modeling accuracy. On the other hand, an optimized T3-FLS with SMC is introduced to eliminate the adaption errors and ensure robustness. Several simulations show that known parameters converge under uncertainty, and the stability is kept, well. Also, output signals follow the desired trajectories under dynamic perturbations, identification errors, and uncertainties.

Keywords Control · Robotic · Intelligent systems · Fuzzy logic · Type-3 fuzzy logic

Introduction

Robotic science is a modern technology that surpasses the constraints of traditional engineering. A comprehensive understanding of robots and their applications necessitates expertise in electrical engineering, mechanical engineering, system engineering, industrial engineering, computer science, and mathematics. One of the specific robotic systems is UAV. UAVs have become increasingly important in a wide range of fields such as surveillance and reconnaissance, environmental monitoring, gathering information in areas that are difficult to access, locating and assisting individuals in distress, agriculture, irrigation management, infrastructure inspection, film and photography, and numerous commercial applications [1, 2]. In general, it can be said that UAVs have attracted a lot of attention in recent decades. The main advantages of UAVs compared to conventional helicopters are:

- Flying robots are easier to design and build than helicopters. Also, it does not require a mechanical connection to change the inclination of the blades.
- Having four smaller rotors than the single rotor of a conventional helicopter allows it to have less kinetic energy and less damage in case of an accidental fall.
- It has a symmetrical structure, and considering that the movement of UAVs is only dependent on the rotation

✉ Amith Khadakar
   amitk@qu.edu.qa

✉ Ardashir Mohammadzadeh
   a.mzadeh@sut.edu.cn

✉ Chunwei Zhang
   zhangchunwei@sut.edu.cn

1 Zhejiang Guangsha Vocational and Technical University of Construction, Dongyang 322100, China

2 Zhejiang Ruiao Testing Technology Service Co., Ltd.,, Hangzhou 310027, China

3 Department of Electrical Engineering, Qatar University, POBOX -2713 Doha, Qatar

4 Multidisciplinary Center for Infrastructure Engineering, Shenyang University of Technology, Shenyang, China

5 Department of Electrical Engineering, University of Bonab, Bonab, Iran

rate, it makes them maneuverable and requires simpler control systems.

UAVs consist of active control systems with 6 degrees of freedom and four independent controllers. They are devices with four rotors, whose translational and rotational movements are created by changes in the speed of the rotors [3]. To control UAVs, the following three features should be considered:

- Variable modes with time-delay.
- Dynamics with uncertainty.
- Multi-input-multi-output and nonlinear structure.

Studying the stability and control of UAVs concerning nonlinear components and disturbances is a challenging problem. Typically, UAVs can be maneuvered using a remote control system and stabilized with an external controller. Attitude control is employed to maintain the optimal position of UAVs. Various control methods, including linear control, non-linear, adaptive, fuzzy, and neural controllers, have been utilized to control the attitude of UAVs. However, controlling UAVs becomes challenging in the presence of uncertainties [4–6].

Literature review

In [7], an adaptive controller is suggested to track the position of the UAV under uncertainty and disturbance. The stability analysis is done using the concept of the Lyapunov scheme. In [8], a control method based on adaptive control and SMC is used to combine the tracking error with the concept of Lyapunov stability. In [9], a tensor transformation model based on SMC is presented. The provided controller is divided into two stages, in the first step, a transformation model is provided, and then, in the second step, the final SMC rule for the time-varying conditions is presented. In [10], a control structure is designed by the feedback linearization approach. The feedback linearization transforms the UAV dynamics into a simple fourth-order linear system, and then SMC is designed. In [11], a hybrid three-axis state control is presented, so that the time-limited SMC is designed to control the three-axis angular rate in the inner loop. Then, a PI based on the linear square regulator is considered to control the rotation angles in the outer ring. In [12], some controllers like fuzzy control, feedback linearization, and SMC have been used for the UAV. In [13], two control methods for the UAV are presented. The first method is designed using PID and the second method is designed on the basis of feedback of nonlinear state and linear matrix inequality. In [14], the dynamic UAV is obtained based on physical laws, then a control method is designed based on the backward design method for the stability of UAV under actuator and sensor errors.

The SMC is known as an effective method for designing a robust controller for high-order systems with uncertainties [15]. The main feature of SMC is less sensitivity to perturbations and changes in system parameters. As a practical example, in [16], an adaptive nonlinear SMC is designed for a robot arm in the presence of uncertainty and disturbance. Also, to demonstrate the effectiveness of the suggested approach, a practical examination is carried out on an inverted pendulum. The paths of the system by the suggested SMC reach to the equilibrium point in a limited time.

The FLSs have good applicability in the control of robotic systems. In some studies, the application of FLSs has been investigated. For instance, a new application of UAVs is introduced in [17] to improve road maintenance on partially erased sidewalk edges. It develops the stabilization and computer vision-based decision-making systems using FLSs. A controller using FLS is implemented in [18] to create a control model in a stable environment, comparing it to conventional control methods. The FLS-based controller approach allows the robot to move easily and efficiently in the test environment, minimizing energy consumption and operating in a flexible scheme. It is shown that the FLS-based controller is faster and more accurate than the traditional methods. An adaptive control scheme using FLSs with Jordan feedback structure is suggested in [19] to address the challenges of operating UAVs in extreme environments. It is shown the FLS strategy can effectively manage system uncertainty and track the reference trajectory with good accuracy, low computational load, and quick convergence rate. The controller's stability is demonstrated using Lyapunov's method. In [20], a fractional-order PID using FLSs is studied for stabilizing a UAV considering the nonlinear dynamics. FLSs are used to adjust parameters under disturbances and uncertainties. The multi-objective thermal optimization is employed to determine controller parameters to minimize control energy and tracking errors. A new quadcopter UAV platform is introduced in [21], and a type-2 (T2) FLS-based controller is designed to improve control robustness and manage computation costs for practical control. The designed system is used to control a UAV and is tested using a software-in-the-loop simulator and actual flight experiments. In [22], some controllers and modeling methods are reviewed and compared. In [23], a fuzzy PID is designed for a line following problem. The controller's gains are chosen online based on changes in position and orientation errors. The results verify that the type-2 FLS-based controller outperforms the convectional fuzzy and PID controllers in stabilization and time-variant trajectory tests.

Recently, type-3 FLSs are widely used for many problems such as: robotic [24, 25], monitoring [26], forecasting [27], electrical vehicles [28, 29], adaptive control systems [30], classification [26], modeling [31], and many others. How-

ever, T3-FLS-based control of UAVs has not been studied, well. The literature review shows that:

- In most controllers, the dynamics of UAVs are considered to be known.
- In a few studies, FLS-based controllers have been developed, but the robustness analyses are neglected.
- In a few SMCs, the robustness is studied, but, the dynamic parameters of UAV are considered constant.
- T3-FLSs based control of UAVs has not been studied, well.

In this paper, a T3-FLS-based controller is developed. The main novelties and contributions are:

- An adaptive scheme is developed for model identification using the input/output data sets.
- New adaptation laws are obtained for dynamic parameters.
- A T3-FLS is developed to compensate for the identification errors.
- The robustness is analyzed considering the adaptation errors

Dynamic modeling

In this research, a UAV with four rotors as shown in Fig. 1 is considered. This UAV consists of a rigid and cross-shaped frame with four propellers. The considered UAV can be moved in certain directions by increasing/reduction of the total propulsion force. If the speed of all four propellers increases or decreases at the same time, vertical movement is created. The rotational movement around the longitudinal axis and the related translational movement are created by
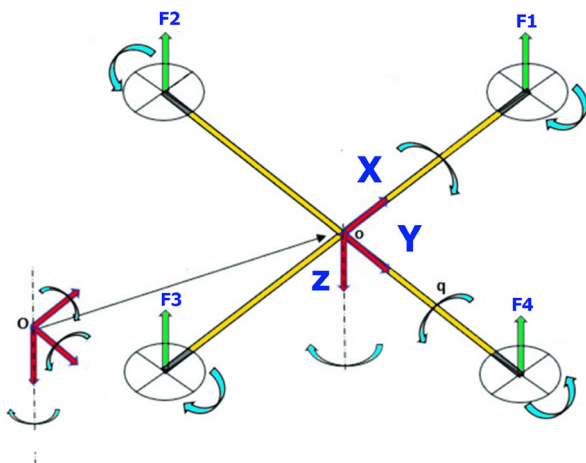

Fig. 1 Schematic of a UAV with four rotors

increasing and decreasing the speed of propellers one and three in reverse. If the speed of propellers two and four is changed inversely, the rotational movement around the transverse axis and also the translational movement related to it are formed. Finally, the rotational movement around the height axis is made from the torque difference between the two pairs of propellers (1, 3) and (2, 4) [32]. In this research, the following assumptions have been considered:

- The structure and propellers are rigid and symmetrical.
- Thrust forces have a proportionality to the square of the rotation speed of the blades.

Based on the above assumptions, the dynamic equations of the aerodynamic forces created by the rotation of the propellers are written as follows based on Newton–Euler equations [33]:

$$
\begin{cases}
m\ddot{\zeta} = F_f + F_d + F_g, \\
J\dot{\Phi} = -\Phi^T J \Phi + \rho_f - \rho_a - \rho_g,
\end{cases}
\tag{1}
$$

while m denotes the total mass of the UAV, ξ is the center of the UAV relative to the inertial frame and a fixed and positive-definite inertial matrix of the UAV is symmetrical to the rigid body. J is defined as follows:

$$
J = \begin{bmatrix} I_\chi & 0 & 0 \\ 0 & I_y & 0 \\ 0 & 0 & I_z \end{bmatrix},
\tag{2}
$$

where I_χ, I_y, I_z represent the inertias related to the χ, y, z axes. Φ shows the angular velocities:

$$
\Phi = \begin{bmatrix} 1 & 0 & -\sin\Theta \\ 0 & \cos\varphi & \cos\Theta\sin\varphi \\ 0 & -\sin\varphi & \cos\varphi\cos\Theta \end{bmatrix} \begin{bmatrix} \dot{\varphi} \\ \dot{\Theta} \\ \dot{\Omega} \end{bmatrix},
\tag{3}
$$

While φ, Θ, and Ω, denote the angles around the longitudinal, transverse, and height axis, respectively. F_f is written as:

$$
F_f = \begin{bmatrix} \cos\varphi\cos\Omega\sin\Theta + \sin\varphi\sin\Omega \\ \cos\varphi\sin\Theta\sin\Omega - \sin\varphi\cos\Omega \\ \cos\varphi\cos\Theta \end{bmatrix} \sum_{i=1}^{4} F_i,
\tag{4}
$$

where $F_i = K_p w_i^2$ and K_p is related to the force and w_i denotes the angular speed of the rotor. The F_d represents the result of the forces produced along the axes χ, y, z:

$$
F_d = \begin{bmatrix} -K_{fdx} & 0 & 0 \\ 0 & -K_{fdy} & 0 \\ 0 & 0 & -K_{fdz} \end{bmatrix} \dot{\zeta},
\tag{5}
$$

where K_{fdz}, K_{fdy}, K_{fdx} are the positive coefficients, respectively. Gravitational force F_g is shown as follows:

$$F_g = \begin{bmatrix} 0 \\ 0 \\ -mg \end{bmatrix}, \tag{6}$$

where ρ_f shows the moment of inertia related to the fixed object:

$$\rho_f = \begin{bmatrix} d(F_3 - F_1) \\ d(F_4 - F_2) \\ C_d(w_1^2 - w_2^2 + w_3^2 - w_4^2) \end{bmatrix}, \tag{7}$$

where d denotes the distance between the center and propellers, and C_d is a coefficient. The torque ρ_a is written as:

$$\rho_a = \begin{bmatrix} K_{fax} & 0 & 0 \\ 0 & K_{fay} & 0 \\ 0 & 0 & K_{faz} \end{bmatrix} \|\Phi\|^2, \tag{8}$$

where K_{faz}, K_{fay}, K_{fax} are aerodynamic friction coefficients. ρ_g means the result of torques created due to the gyroscopic effect:

$$\rho_g = \sum_{i=1}^{4} \Phi^T J_r \begin{bmatrix} 0 \\ 0 \\ (-1)^{i+1} w_i \end{bmatrix}, \tag{9}$$

where J_r denotes the inertia of rotor. The relationship between the controllers and the velocities is:

$$\begin{bmatrix} u_1 \\ u_2 \\ u_3 \\ u_4 \end{bmatrix} = \begin{bmatrix} K_p & K_p & K_p & K_p \\ -K_p & 0 & K_p & 0 \\ 0 & -K_p & 0 & K_p \\ C_D & -C_D & C_D & -C_D \end{bmatrix} \begin{bmatrix} w_1^2 \\ w_2^2 \\ w_3^2 \\ w_4^2 \end{bmatrix}, \tag{10}$$

where u_i, $i = 1, ..., 4$ are control inputs. The velocities w_i $(i = 1, ..., 4)$ can be written as follows:

$$\begin{bmatrix} w_1 \\ w_2 \\ w_3 \\ w_4 \end{bmatrix} = \left(\begin{bmatrix} K_p & K_p & K_p & K_p \\ -K_p & 0 & K_p & 0 \\ 0 & -K_p & 0 & K_p \\ C_D & -C_D & C_D & -C_D \end{bmatrix}^{-1} \begin{bmatrix} u_1 \\ u_2 \\ u_3 \\ u_4 \end{bmatrix} \right)^{\frac{1}{2}}. \tag{11}$$

As a result, the dynamic of UAV is determined as:

$$\ddot{\chi} = \frac{1}{m} \left[-K_{fdx}\dot{\chi} + (cos\varphi \sin \Theta \cos \Omega + \sin \varphi \sin \Omega)u_1 \right],$$

$$\ddot{y} = \frac{1}{m} \left[-K_{fdy}\dot{y} + (cos\varphi \sin \Theta \sin \Omega - \sin \varphi \cos \Omega)u_1 \right],$$

$$\ddot{z} = \frac{1}{m} \left[-K_{fdz}\dot{z} + (cos\varphi \cos \Theta)u_1 \right] - g,$$

$$\ddot{\varphi} = \frac{1}{I_\chi} \left[(I_y - I_z)\dot{\Omega}\dot{\Theta} - K_{fax}\dot{\varphi}^2 - J_r \bar{\Phi}\dot{\Theta} + du_2 \right],$$

$$\ddot{\Theta} = \frac{1}{I_y} \left[(I_z - I_\chi)\dot{\Omega}\dot{\varphi} - K_{fay}\dot{\Theta}^2 + J_r \bar{\Phi}\dot{\varphi} + du_3 \right],$$

$$\ddot{\Omega} = \frac{1}{I_z} \left[(I_\chi - I_y)\dot{\varphi}\dot{\Theta} - K_{faz}\dot{\Omega}^2 + C_D u_4 \right], \tag{12}$$

where $\bar{\Phi} = w_1 - w_2 + w_3 - w_4$. The considered UAV is fully actuated with four control inputs, which are used to control φ, Θ, Ω, and z. Assume that $X = \begin{bmatrix} \varphi, \dot{\varphi}, \Theta, \dot{\Theta}, \Omega, \dot{\Omega}, z, \dot{z} \end{bmatrix}^T$ and $U = [u_2, u_3, u_4, u_1]^T$ denote the state and the controller vectors. The dynamic model considered in (12) based on the state space model is expressed as follows:

$$\dot{X} = F(\chi) + G(\chi)U \tag{13}$$

where F and G are written as:

$$F(\chi) = \begin{bmatrix} \chi_2 \\ a_1\chi_4\chi_6 + a_2\chi_2^2 + a_3\bar{\Phi}\chi_4 \\ \chi_4 \\ a_4\chi_2\chi_6 + a_5\chi_4^2 + a_6\bar{\Phi}\chi_2 \\ \chi_6 \\ a_7\chi_2\chi_4 + a_8\chi_6^2 \\ \chi_8 \\ a_9\chi_8 - g \end{bmatrix} \tag{14}$$

$$G(\chi) = \begin{bmatrix} 0 & 0 & 0 & 0 \\ b_1 & 0 & 0 & 0 \\ 0 & 0 & 0 & 0 \\ 0 & b_2 & 0 & 0 \\ 0 & 0 & 0 & 0 \\ 0 & 0 & b_3 & 0 \\ 0 & 0 & 0 & 0 \\ 0 & 0 & 0 & \frac{\cos \chi_1 \cos \chi_3}{m} \end{bmatrix} \tag{15}$$

where

$$a_1 = \frac{I_y - I_z}{I_\chi}, \ a_2 = \frac{-K_{fax}}{I_\chi}, \ a_3 = \frac{-J_r}{I_\chi}, \ a_4 = \frac{I_z - I_\chi}{I_y}$$

$$a_5 = \frac{-K_{fay}}{I_y}, \ a_6 = \frac{J_r}{I_y}, \ a_7 = \frac{I_\chi - I_y}{I_z}, \ a_9 = \frac{-K_{fdz}}{m},$$

$$b_1 = \frac{d}{I_\chi}, \ b_2 = \frac{d}{I_y}, \ b_3 = \frac{C_D}{I_z} \tag{16}$$

The following lemma is considered in the analysis.

Lemma 1 *Suppose a definite positive function $V(t)$ satisfies:*

$$\dot{V}(t) \leq -\beta V(t) - \alpha V^{\gamma}(t) \tag{17}$$

where α/β are positive, $0 < a < b$, and $\gamma = \frac{a}{b}$, then $V(t)$ in limited time (18) is converged to zero.

$$t_s = t_0 + \frac{1}{\beta(1-\gamma)} \ln\left(\frac{\beta V^{1-\gamma}(t_0) + \alpha}{\alpha}\right). \tag{18}$$

The designed control scheme is shown in Fig. 2. First, an adaptive model is identified for the plant using the input/output info, and then a SMC is designed. A T3-FLS is used to estimate the disturbances and identification errors.

Type-3 fuzzy systems

Type-2 extensions of traditional type-1 fuzzy systems, which are used in fuzzy logic to model uncertainty and imprecision in decision-making processes. These systems are particularly useful in situations where the uncertainty in the input data is high or where the decision-making process is complex. T2-FLSs allow for the representation of higher levels of uncertainty compared to type-1 FLSs. In a type-2 fuzzy system, each linguistic variable is associated with a fuzzy set that has a membership function that is itself a fuzzy set. This allows for the modeling of uncertainty in both the membership grade and the shape of the membership function. T2-FLSs are useful in situations where the uncertainty in the input data is not well understood or where there is a need to model varying levels of uncertainty.

T3-FLSs are an even more advanced extension of type-1 and type-2 FLSs. In a T3-FLS, each linguistic variable is associated with a fuzzy set that has a membership function that is a type-2 fuzzy set. This allows for the representation of even higher levels of uncertainty and complexity in the decision-making process. Type-3 fuzzy systems are particularly useful in situations where the uncertainty in the input data is extremely high or where there is a need to model complex relationships between variables. These systems offer a powerful tool for dealing with uncertainty and imprecision in complex decision-making processes, making them valuable tools for researchers and practitioners in a variety of domains. In this paper, T3-FLSs are used to estimate the disturbances and nonlinearities. The computations are summarized as follows (see Fig. 3): 1) The inputs are the states of plant χ_i, $i = 1, ..., n$.

2) The memberships $\bar{q}_{\tilde{\Psi}_i^j|\bar{\lambda}_k}$, $\bar{q}_{\tilde{\Psi}_i^j|\underline{\lambda}_k}$, $\underline{q}_{\tilde{\Psi}_i^j|\bar{\lambda}_k}$, and $\underline{q}_{\tilde{\Psi}_i^j|\underline{\lambda}_k}$ for $\tilde{\Psi}_i^j$ (j-th membership function (MF) for χ_i, $i = 1, 2$) are obtained as (see Fig. 4):

$$\bar{q}_{\tilde{\Psi}_i^j|\bar{\lambda}_k} = \begin{cases} 1 - \left(\dfrac{\left|\chi_i - \bar{\chi}_{\tilde{\Psi}_i^j}\right|}{\underline{\sigma}_{\tilde{\Psi}_i^j}}\right)^{\bar{\lambda}_k} & \text{if } \bar{\chi}_{\tilde{\Psi}_i^j} - \underline{\sigma}_{\tilde{\Psi}_i^j} < \chi_i \leq \bar{\chi}_{\tilde{\Psi}_i^j} \\[4mm] 1 - \left(\dfrac{\left|\chi_i - \bar{\chi}_{\tilde{\Psi}_i^j}\right|}{\bar{\sigma}_{\tilde{\Psi}_i^j}}\right)^{\bar{\lambda}_k} & \text{if } \bar{\chi}_{\tilde{\Psi}_i^j} < \chi_i \leq \bar{\chi}_{\tilde{\Psi}_i^j} + \bar{\sigma}_{\tilde{\Psi}_i^j} \\[4mm] 0 & \text{if } \chi_i > \bar{\chi}_{\tilde{\Psi}_i^j} + \bar{\sigma}_{\tilde{\Psi}_i^j} \text{ or } \chi_i \leq \bar{\chi}_{\tilde{\Psi}_i^j} - \underline{\sigma}_{\tilde{\Psi}_i^j} \end{cases} \tag{19}$$

$$\bar{q}_{\tilde{\Psi}_i^j|\underline{\lambda}_k} = \begin{cases} 1 - \left(\dfrac{\left|\chi_i - \bar{\chi}_{\tilde{\Psi}_i^j}\right|}{\underline{\sigma}_{\tilde{\Psi}_i^j}}\right)^{\underline{\lambda}_k} & \text{if } \bar{\chi}_{\tilde{\Psi}_i^j} - \underline{\sigma}_{\tilde{\Psi}_i^j} < \chi_i \leq \bar{\chi}_{\tilde{\Psi}_i^j} \\[4mm] 1 - \left(\dfrac{\left|\chi_i - \bar{\chi}_{\tilde{\Psi}_i^j}\right|}{\bar{\sigma}_{\tilde{\Psi}_i^j}}\right)^{\underline{\lambda}_k} & \text{if } \bar{\chi}_{\tilde{\Psi}_i^j} < \chi_i \leq \bar{\chi}_{\tilde{\Psi}_i^j} + \bar{\sigma}_{\tilde{\Psi}_i^j} \\[4mm] 0 & \text{if } \chi_i > \bar{\chi}_{\tilde{\Psi}_i^j} + \bar{\sigma}_{\tilde{\Psi}_i^j} \text{ or } \chi_i \leq \bar{\chi}_{\tilde{\Psi}_i^j} - \underline{\sigma}_{\tilde{\Psi}_i^j} \end{cases} \tag{20}$$

$$\underline{q}_{\tilde{\Psi}_i^j|\bar{\lambda}_k} = \begin{cases} 1 - \left(\dfrac{\left|\chi_i - \bar{\chi}_{\tilde{\Psi}_i^j}\right|}{\underline{\sigma}_{\tilde{\Psi}_i^j}}\right)^{\frac{1}{\bar{\lambda}_k}} & \text{if } \bar{\chi}_{\tilde{\Psi}_i^j} - \underline{\sigma}_{\tilde{\Psi}_i^j} < \chi_i \leq \bar{\chi}_{\tilde{\Psi}_i^j} \\[4mm] 1 - \left(\dfrac{\left|\chi_i - \bar{\chi}_{\tilde{\Psi}_i^j}\right|}{\bar{\sigma}_{\tilde{\Psi}_i^j}}\right)^{\frac{1}{\bar{\lambda}_k}} & \text{if } \bar{\chi}_{\tilde{\Psi}_i^j} < \chi_i \leq \bar{\chi}_{\tilde{\Psi}_i^j} + \bar{\sigma}_{\tilde{\Psi}_i^j} \\[4mm] 0 & \text{if } \chi_i > \bar{\chi}_{\tilde{\Psi}_i^j} + \bar{\sigma}_{\tilde{\Psi}_i^j} \text{ or } \chi_i \leq \bar{\chi}_{\tilde{\Psi}_i^j} - \underline{\sigma}_{\tilde{\Psi}_i^j} \end{cases} \tag{21}$$

$$\underline{q}_{\tilde{\Psi}_i^j|\underline{\lambda}_k} = \begin{cases} 1 - \left(\dfrac{\left|\chi_i - \bar{\chi}_{\tilde{\Psi}_i^j}\right|}{\underline{\sigma}_{\tilde{\Psi}_i^j}}\right)^{\frac{1}{\underline{\lambda}_k}} & \text{if } \bar{\chi}_{\tilde{\Psi}_i^j} - \underline{\sigma}_{\tilde{\Psi}_i^j} < \chi_i \leq \bar{\chi}_{\tilde{\Psi}_i^j} \\[4mm] 1 - \left(\dfrac{\left|\chi_i - \bar{\chi}_{\tilde{\Psi}_i^j}\right|}{\bar{\sigma}_{\tilde{\Psi}_i^j}}\right)^{\frac{1}{\underline{\lambda}_k}} & \text{if } \bar{\chi}_{\tilde{\Psi}_i^j} < \chi_i \leq \bar{\chi}_{\tilde{\Psi}_i^j} + \bar{\sigma}_{\tilde{\Psi}_i^j} \\[4mm] 0 & \text{if } \chi_i > \bar{\chi}_{\tilde{\Psi}_i^j} + \bar{\sigma}_{\tilde{\Psi}_i^j} \text{ or } \chi_i \leq \bar{\chi}_{\tilde{\Psi}_i^j} - \underline{\sigma}_{\tilde{\Psi}_i^j} \end{cases} \tag{22}$$

where $\bar{\lambda}_k/\underline{\lambda}_k$ represent the upper/lower slices.

3) The rule firings $\bar{\ell}_{\bar{\lambda}_k}^l$, $\bar{\ell}_{\underline{\lambda}_k}^l$, $\underline{\ell}_{\bar{\lambda}_k}^l$, and $\underline{\ell}_{\underline{\lambda}_k}^l$ are written as

$$\bar{\ell}_{\bar{\lambda}_k}^l = \bar{q}_{\tilde{\Psi}_1^{x_1}|\bar{\lambda}_k} \cdot \bar{q}_{\tilde{\Psi}_1^{x_2}|\bar{\lambda}_k} \cdots \bar{q}_{\tilde{\Psi}_1^{x_n}|\bar{\lambda}_k} \tag{23}$$

$$\bar{\ell}_{\underline{\lambda}_k}^l = \bar{q}_{\tilde{\Psi}_1^{x_1}|\underline{\lambda}_k} \cdot \bar{q}_{\tilde{\Psi}_1^{x_2}|\underline{\lambda}_k} \cdots \bar{q}_{\tilde{\Psi}_1^{x_n}|\underline{\lambda}_k} \tag{24}$$

$$\underline{\ell}_{\bar{\lambda}_k}^l = \underline{q}_{\tilde{\Psi}_1^{x_1}|\bar{\lambda}_k} \cdot \underline{q}_{\tilde{\Psi}_1^{x_2}|\bar{\lambda}_k} \cdots \underline{q}_{\tilde{\Psi}_1^{x_n}|\bar{\lambda}_k} \tag{25}$$
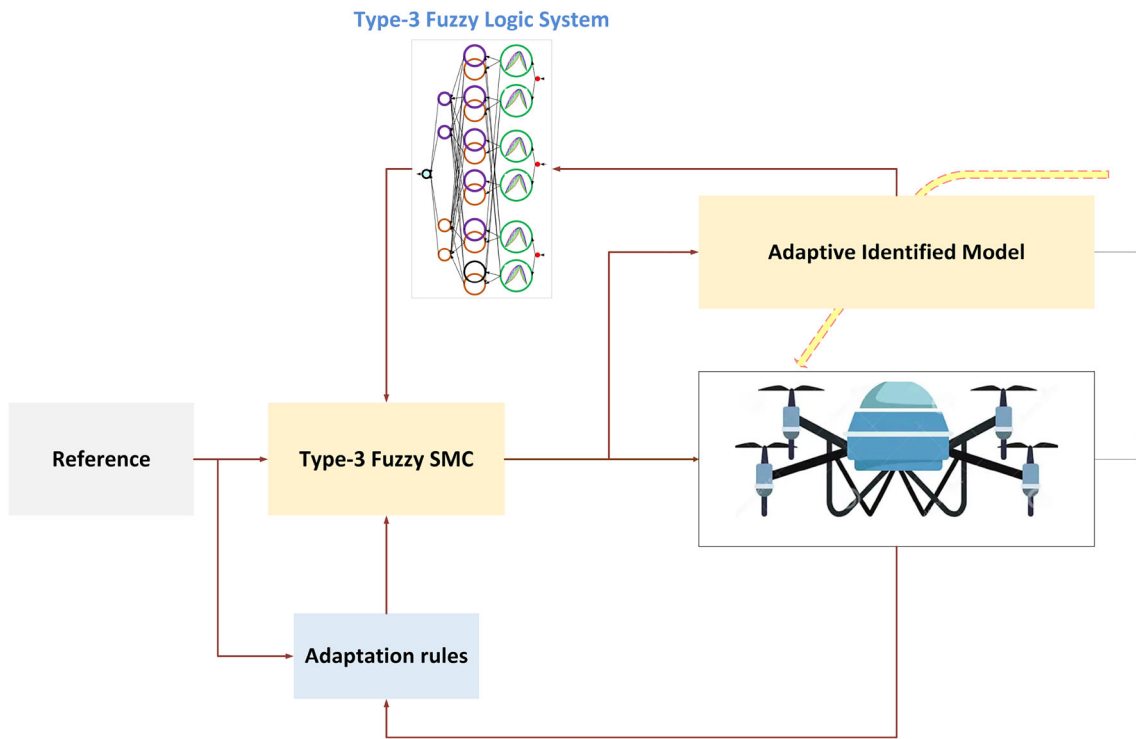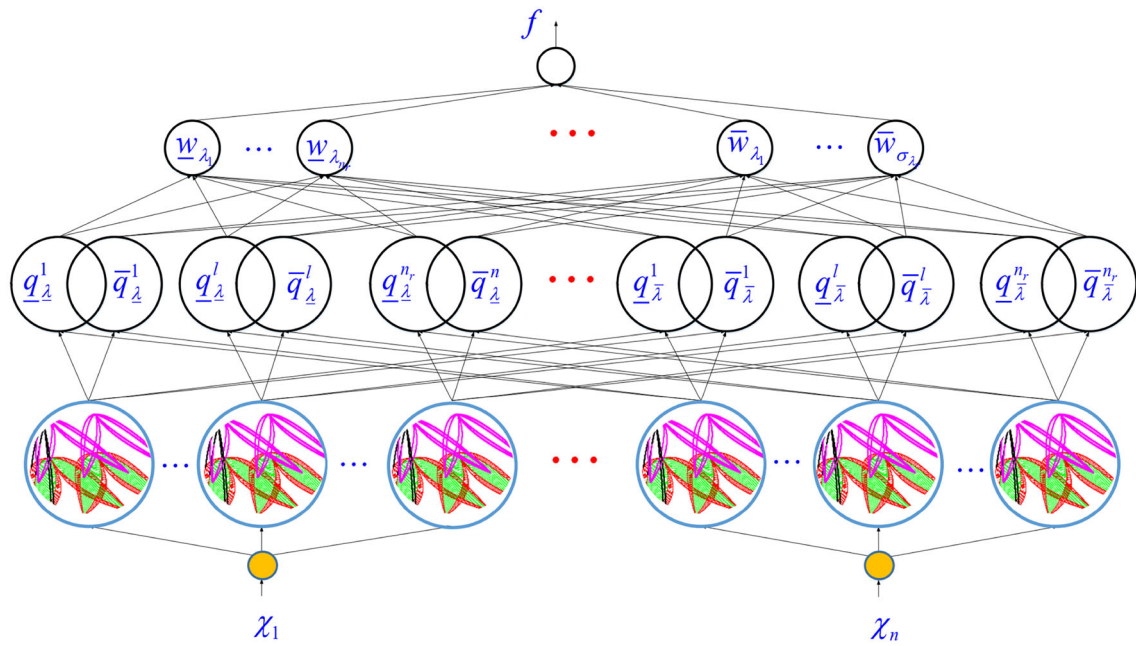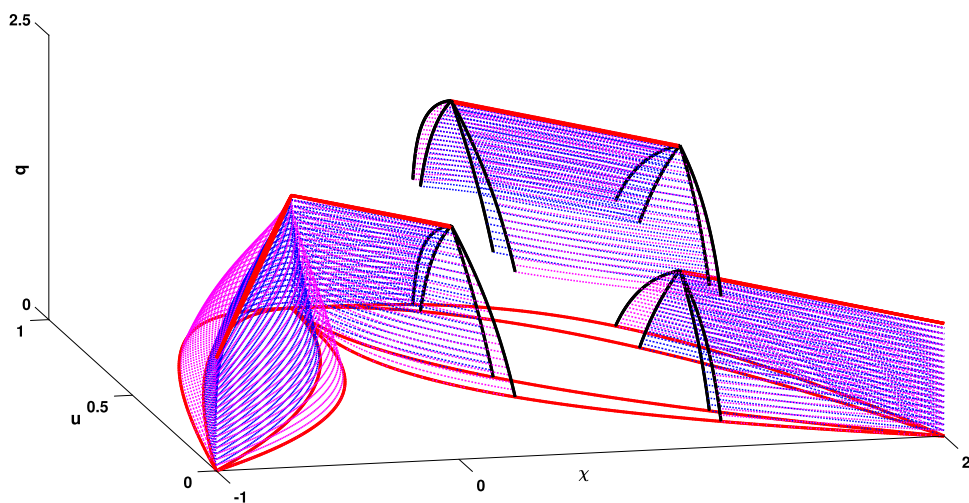
Fig. 2 Designed control scheme

Fig. 3 Schematic of T3-FLS

Fig. 4 Membership functions

$$\ell^l_{\underline{\lambda}_k} = \underline{q}_{\tilde{\Psi}^{x_1}_1|\underline{\lambda}_k} \cdot \underline{q}_{\tilde{\Psi}^{x_2}_1|\underline{\lambda}_k} \cdots \underline{q}_{\tilde{\Psi}^{x_n}_1|\underline{\lambda}_k} \tag{26}$$

4) The output is given as:

$$f = \sum_{k=1}^{K} \left(\underline{\lambda}_k \underline{G}_k + \bar{\lambda}_k \bar{G}_k\right) \bigg/ \sum_{k=1}^{K} \left(\underline{\lambda}_k + \bar{\lambda}_k\right) \tag{27}$$

where,

$$\bar{G}_k = \frac{\sum_{l=1}^{q} \left(\bar{\ell}^l_{\bar{\lambda}_k} \bar{w}_l + \underline{\ell}^l_{\bar{\lambda}_k} \underline{w}_l\right)}{\sum_{l=1}^{q} \left(\bar{\ell}^l_{\bar{\lambda}_k} + \underline{\ell}^l_{\bar{\lambda}_k}\right)} \tag{28}$$

$$\underline{G}_k = \frac{\sum_{l=1}^{q} \left(\bar{\ell}^l_{\underline{\lambda}_k} \bar{w}_l + \underline{\ell}^l_{\underline{\lambda}_k} \underline{w}_l\right)}{\sum_{l=1}^{q} \left(\bar{\ell}^l_{\underline{\lambda}_k} + \underline{\ell}^l_{\underline{\lambda}_k}\right)} \tag{29}$$

Control

In this section, the control is designed and analyzed. The main results are summarized in Theorem 2. The output vector is $y = [\varphi, \Theta, \Omega, z]^T$, then the errors are defined as follows:

$$\begin{cases} e_{\varphi_1} = y_1 - \varphi_d \\ e_{\varphi_2} = \dot{y}_1 - \dot{\varphi}_d \end{cases} \quad \begin{cases} e_{\Theta_1} = y_2 - \Theta_d \\ e_{\Theta_2} = \dot{y}_2 - \dot{\Theta}_d \end{cases}$$
$$\begin{cases} e_{\Omega_1} = y_3 - \Omega_d \\ e_{\Omega_2} = \dot{y}_3 - \dot{\Omega}_d \end{cases} \quad \begin{cases} e_{z_1} = y_4 - z_d \\ e_{z_2} = \dot{y}_4 - \dot{z}_d \end{cases} \tag{30}$$

where $y_d = [\varphi_d, \Theta_d, \Omega_d, z_d]^T$ is the reference output. The sliding surface is defined as:

$$s_1 = e_{\varphi_2} + \alpha'_1 e_{\varphi_1} + k_1 \int_0^t s_1(\tau)d\tau,$$

$$s_2 = e_{\Theta_2} + \alpha'_2 e_{\Theta_1} + k_2 \int_0^t s_2(\tau)d\tau,$$

$$s_3 = e_{\Omega_2} + \alpha'_3 e_{\Omega_1} + k_3 \int_0^t s_3(\tau)d\tau,$$

$$s_4 = e_{z_2} + \alpha'_4 e_{z_1} + k_4 \int_0^t s_4(\tau)d\tau, \tag{31}$$

where $\alpha_l', k_l, l = 1, ..., 4$ are positive constants. By taking derivative from (31), we can write:

$$\begin{aligned} \dot{s}_1 &= \dot{e}_{\varphi_2} + \alpha'_1 \dot{e}_{\varphi_1} + k_1 s_1 \\ &= a_1 \chi_4 \chi_6 + a_2 \chi_2^2 + a_3 \bar{\Phi} \chi_4 \\ &\quad + b_1 u_2 - \ddot{\varphi}_d + \alpha'_1 \dot{e}_{\varphi_1} + k_1 s_1, \\ \dot{s}_2 &= \dot{e}_{\Theta_2} + \alpha'_2 \dot{e}_{\Theta_1} + k_2 s_2 \\ &= a_5 \chi_4^2 + \bar{\Phi} a_6 \chi_2 + b_2 u_3 + \chi_2 a_4 \chi_6 \\ &\quad - \ddot{\Theta}_d + \alpha'_2 \dot{e}_{\Theta_1} + k_2 s_2, \\ \dot{s}_3 &= \dot{e}_{\Omega_2} + \alpha'_3 \dot{e}_{\Omega_1} + k_3 s_3 \\ &= a_7 \chi_2 \chi_4 + a_8 \chi_6^2 + b_3 u_4 - \ddot{\Omega}_d + \alpha'_3 \dot{e}_{\Omega_1} + k_3 s_3, \\ \dot{s}_4 &= \dot{e}_{z_2} + \alpha'_4 \dot{e}_{z_1} + k_4 s_4 \\ &= a_9 \chi_8 - g + \frac{\cos \chi_1 \cos \chi_3}{m} u_1 - \ddot{z}_d + \alpha'_4 \dot{e}_{z_1} + k_4 s_4. \end{aligned} \tag{32}$$

Theorem 2 *Considering the dynamic model as (13), sliding surfaces as (31), controllers (33), and adaptation laws (36)–(40), the robot in a limited time is reached to the target position.*

The controllers are given as:

$$
\begin{aligned}
u_2 &= -f_2(\chi, w_2) - \hat{\varsigma}_1 \chi_4 \chi_6 - \hat{\varsigma}_2 \chi_2^2 - \hat{\varsigma}_3 \bar{\Phi} \chi_4 + \hat{h}_1 \kappa_1, \\
u_3 &= -f_3(\chi, w_3) - \hat{\varsigma}_4 \chi_2 \chi_6 - \hat{\varsigma}_5 \chi_4^2 - \hat{\varsigma}_6 \bar{\Phi} \chi_2 + \hat{h}_2 \kappa_2, \\
u_4 &= -f_4(\chi, w_4) - \hat{\varsigma}_7 \chi_2 \chi_4 - \hat{\varsigma}_8 \chi_6^2 + \hat{h}_3 \kappa_3, \\
u_1 &= -f_1(\chi, w_1) + \frac{1}{\cos x_1 \cos x_3}[-\hat{\varsigma}_9 \chi_8 + \hat{m} \kappa_4],
\end{aligned}
\tag{33}
$$

where $\hat{\varsigma}_i$ $(i = 1, ..., 9)$, $\hat{h}_j$ $(j = 1, 2, 3)$ and $\hat{m}$ are the estimation of:

$$
\varsigma_1 = \frac{a_1}{b_1}, \varsigma_2 = \frac{a_2}{b_1}, \varsigma_3 = \frac{a_3}{b_1}, \varsigma_4 = \frac{a_4}{b_2}, \varsigma_5 = \frac{a_5}{b_2}
$$

$$
\varsigma_6 = \frac{a_6}{b_2}, \varsigma_7 = \frac{a_7}{b_3}, \varsigma_8 = \frac{a_8}{b_3}, \varsigma_9 = m a_9, h_1 = \frac{1}{b_1}
\tag{34}
$$

$$
h_2 = \frac{1}{b_2}, h_3 = \frac{1}{b_3}
$$

κ_r $(r = 1, ..., 4)$ are written as:

$$
\begin{aligned}
\kappa_1 &= -\alpha_1' \dot{e}_{\varphi_1} - k_1 s_1 + \ddot{\varphi}_d, \\
\kappa_2 &= -\alpha_2' \dot{e}_{\Theta_1} - k_2 s_2 + \ddot{\Theta}_d, \\
\kappa_3 &= \ddot{\Omega}_d - \alpha_3' \dot{e}_{\Omega_1} - k_3 s_3, \\
\kappa_4 &= g - \alpha_4' \dot{e}_{z_1} - k_4 s_4 + \ddot{z}_d
\end{aligned}
\tag{35}
$$

The adaptation laws are written as:

$$
\begin{cases}
\dot{\hat{\varsigma}}_1 = \alpha_1 \text{sgn}\left(\frac{\partial s_1}{\partial u_2}\right) \chi_4 \chi_6 s_1^{\vartheta} \\
\dot{\hat{\varsigma}}_2 = \alpha_1 \text{sgn}\left(\frac{\partial s_1}{\partial u_2}\right) \chi_2^2 s_1^{\vartheta} \\
\dot{\hat{\varsigma}}_3 = \alpha_1 \text{sgn}\left(\frac{\partial s_1}{\partial u_2}\right) \bar{\Phi} \chi_4 s_1^{\vartheta} \\
\dot{\hat{h}}_1 = -\beta_1 \text{sgn}\left(\frac{\partial s_1}{\partial u_2}\right) \kappa_1 s_1
\end{cases}
\tag{36}
$$

$$
\begin{cases}
\dot{\hat{\varsigma}}_4 = \alpha_2 \text{sgn}\left(\frac{\partial s_2}{\partial u_3}\right) \chi_2 \chi_6 s_2^{\vartheta} \\
\dot{\hat{\varsigma}}_5 = \alpha_2 \text{sgn}\left(\frac{\partial s_2}{\partial u_3}\right) \chi_4^2 s_2^{\vartheta} \\
\dot{\hat{\varsigma}}_6 = \alpha_2 \text{sgn}\left(\frac{\partial s_2}{\partial u_3}\right) \bar{\Phi} \chi_2 s_2^{\vartheta} \\
\dot{\hat{h}}_2 = -\beta_2 \text{sgn}\left(\frac{\partial s_2}{\partial u_3}\right) \kappa_2 s_2
\end{cases}
\tag{37}
$$

$$
\begin{cases}
\dot{\hat{\varsigma}}_7 = \alpha_3 \text{sgn}\left(\frac{\partial s_3}{\partial u_4}\right) \chi_2 \chi_4 s_3^{\vartheta} \\
\dot{\hat{\varsigma}}_8 = \alpha_3 \text{sgn}\left(\frac{\partial s_3}{\partial u_4}\right) \chi_6^2 s_3^{\vartheta} \\
\dot{\hat{h}}_3 = -\beta_3 \text{sgn}\left(\frac{\partial s_3}{\partial u_4}\right) \kappa_3 s_3
\end{cases}
\tag{38}
$$

$$
\begin{cases}
\dot{\hat{\varsigma}}_9 = \alpha_4 \text{sgn}\left(\frac{\partial s_4}{\partial u_1}\right) \chi_8 \cos \chi_1 \cos \chi_3 s_4^{\vartheta} \\
\dot{\hat{m}} = -\beta_4 \text{sgn}\left(\frac{\partial s_4}{\partial u_1}\right) \kappa_4 \cos \chi_1 \cos \chi_3 s_4
\end{cases}
\tag{39}
$$

$$
\dot{w}_i = \text{sgn}\left(\frac{\partial s_i}{\partial u_2}\right) s_i \xi_i
\tag{40}
$$

Proof Consider the V_1 as:

$$
V_1 = \frac{1}{2} s_1^2
\tag{41}
$$

Time derivative of V_1 yields:

$$
\begin{aligned}
\frac{dV_1}{dt} = &\frac{\partial V_1}{\partial s_1} \frac{\partial s_1}{\partial u_2} \frac{\partial u_2}{\partial \hat{\varsigma}_1} \frac{\partial \hat{\varsigma}_1}{\partial t} + \frac{\partial V_1}{\partial s_1} \frac{\partial s_1}{\partial u_2} \frac{\partial u_2}{\partial \hat{\varsigma}_2} \frac{\partial \hat{\varsigma}_2}{\partial t} \\
&+ \frac{\partial V_1}{\partial s_1} \frac{\partial s_1}{\partial u_2} \frac{\partial u_2}{\partial \hat{\varsigma}_3} \frac{\partial \hat{\varsigma}_3}{\partial t} + \frac{\partial V_1}{\partial s_1} \frac{\partial s_1}{\partial u_2} \frac{\partial u_2}{\partial \hat{h}_1} \frac{\partial \hat{h}_1}{\partial t} \\
&+ \frac{\partial V_1}{\partial s_1} \frac{\partial s_1}{\partial u_2} \frac{\partial u_2}{\partial w_2} \frac{\partial w_2}{\partial t}
\end{aligned}
\tag{42}
$$

From the adaptation laws (36)–(40), we have:

$$
\begin{aligned}
\frac{dV_1}{dt} = &s_1 \frac{\partial s_1}{\partial u_2}(-\chi_4 \chi_6) \alpha_1 \text{sgn}\left(\frac{\partial s_1}{\partial u_2}\right) \chi_4 \chi_6 s_1^{\vartheta} \\
&+ s_1 \frac{\partial s_1}{\partial u_2}(-\chi_2^2) \alpha_1 \text{sgn}\left(\frac{\partial s_1}{\partial u_2}\right) \chi_2^2 s_1^{\vartheta} \\
&+ s_1 \frac{\partial s_1}{\partial u_2}(-\bar{\Phi} \chi_4) \alpha_1 \text{sgn}\left(\frac{\partial s_1}{\partial u_2}\right) \bar{\Phi} \chi_4 s_1^{\vartheta} \\
&+ s_1 \frac{\partial s_1}{\partial u_2} \kappa_1 (-\beta_1) \text{sgn}\left(\frac{\partial s_1}{\partial u_2}\right) \kappa_1 s_1 \\
&- s_1 \frac{\partial s_1}{\partial u_2}\left(\xi_1^T\right) \text{sgn}\left(\frac{\partial s_1}{\partial u_2}\right) s_1 \xi_1
\end{aligned}
\tag{43}
$$

From the fact that $\text{sgn}(\frac{\partial s_1}{\partial u_2}) = \left|\frac{\partial s_1}{\partial u_2}\right| / \frac{\partial s_1}{\partial u_2}$, we can write:

$$
\begin{aligned}
\frac{dV_1}{dt} = &-\alpha_1 \left|\frac{\partial s_1}{\partial u_2}\right| (\chi_4 \chi_6)^2 s_1^{\vartheta+1} - \alpha_1 \left|\frac{\partial s_1}{\partial u_2}\right| \chi_2^4 s_1^{\vartheta+1} \\
&- \alpha_1 \left|\frac{\partial s_1}{\partial u_2}\right| (\bar{\Phi} \chi_4)^2 s_1^{\vartheta+1} - \beta_1 (\kappa_1)^2 \left|\frac{\partial s_1}{\partial u_2}\right| s_1^2 \\
&- \alpha_1 \left|\frac{\partial s_1}{\partial u_2}\right| s_1^2 \xi_1^T \xi_1
\end{aligned}
\tag{44}
$$

The equation (44) is simplified as:

$$
\begin{aligned}
\frac{dV_1}{dt} = &-\alpha_1((\chi_4 \chi_6)^2 + \chi_2^4 + (\bar{\Phi} \chi_4)^2) \left|\frac{\partial s_1}{\partial u_2}\right| s_1^{\vartheta+1} \\
&- \beta_1 (\kappa_1)^2 \left|\frac{\partial s_1}{\partial u_2}\right| s_1^2 - \alpha_1 \left|\frac{\partial s_1}{\partial u_2}\right| s_1^2 \xi_1^T \xi_1
\end{aligned}
\tag{45}
$$

Table 1 Control effects of different controllers under different structural conditions

Parameters	Unit	Values
m	Kg	0.486
d	m	0.25
I_χ	N.m/rad/s^2	3.8277e$-$3
I_y		3.8277e$-$3
I_z		7.6565e$-$3
K_{fax}	N/rad/s	5.5671e$-$4
K_{fay}		5.5671e$-$4
K_{faz}		6.3541e$-$4
K_{fdx}	N/m/s	5.5671e$-$4
K_{fsy}		5.5671e$-$4
K_{fdz}		6.3541e$-$4
K_{fpax}	N.m /rad/s	2.9843e$-$3
Cd		3.2321e$-$2
J_r	N.m/rad/s^2	2.8386e$-$5

From (45), we have:

$$\frac{\partial V_1}{\partial t} = -((\chi_4 \chi_6)^2 + \chi_2{}^4 + (\bar{\Phi}\chi_4)^2) 2^{\frac{\vartheta+1}{2}} \left| \frac{\partial s_1}{\partial u_2} \right| \alpha_1 V_1{}^{\frac{\vartheta+1}{2}}$$
$$- 2\alpha_1 \xi_1^T \xi_1 \left| \frac{\partial s_1}{\partial u_2} \right| V_1 - 2\beta_1 (\kappa_1)^2 \left| \frac{\partial s_1}{\partial u_2} \right| V_1 \tag{46}$$

By defining $\gamma = \frac{\vartheta+1}{2}$, it is concluded that:

$$\frac{dV_1}{dt} = -(\chi_2{}^4 + (\chi_4 \chi_6)^2 + (\chi_4 \bar{\Phi})^2) 2^\gamma \left| \frac{\partial s_1}{\partial u_2} \right| \alpha_1 V_1{}^\gamma$$
$$- 2 \left| \frac{\partial s_1}{\partial u_2} \right| V_1 \kappa_1{}^2 \beta_1 - 2\alpha_1 \xi_1^T \xi_1 \left| \frac{\partial s_1}{\partial u_2} \right| V_1 \tag{47}$$

There are μ_1 and μ_2 such that:

$$\dot{V}_1 \leq -\mu_1 V_1{}^\gamma - \mu_2 V_1 \tag{48}$$

where

$$\mu_1 \leq 2^\gamma \alpha_1 \left| \frac{\partial s_1}{\partial u_2} \right| \left[(\chi_4 \chi_6)^2 + (\bar{\Phi}\chi_4)^2 + \chi_2{}^4 \right]$$
$$\mu_2 \leq 2\kappa_1{}^2 \beta_1 \left| \frac{\partial s_1}{\partial u_2} \right| \tag{49}$$

From Lemma 1, the convergence time is computed as follows. First, the both side of (48) is divided by $V_1{}^\gamma$:

$$V_1{}^{-\gamma} \dot{V}_1 \leq -\mu_1 - \mu_2 V_1{}^{1-\gamma} \tag{50}$$

Some computations result in:

$$dt \leq -\frac{V_1{}^{-\gamma}}{\mu_1 + \mu_2 V_1{}^{1-\gamma}} dV_1 \tag{51}$$

Now, by taking integral from (51) at range $[t_0 - t_{s_1}]$, we have:

$$t_{s_1} - t_0 \leq \frac{1}{\mu_2(1-\gamma)} \ln \left(\frac{\mu_1 + \mu_2 V_1(t_0)^{1-\gamma}}{\mu_1} \right) \tag{52}$$

Then, t_{s_1} is obtained as:

$$t_{s_1} = t_0 + \frac{1}{\mu_2(1-\gamma)} \ln \left(\frac{\mu_2 V_1{}^{1-\gamma}(t_0) + \mu_1}{\mu_1} \right) \tag{53}$$

The proof is completed. The other controllers are obtained in the same scheme, just the computations of $\dot{\hat{\varsigma}}_9$ and $\dot{\hat{m}}$ are different. Consider V_4 as:

$$V_4 = \frac{1}{2} s_4{}^2 \tag{54}$$

By taking time-derivative, we have:

$$\frac{dV_4}{dt} = \frac{\partial V_4}{\partial s_4} \frac{\partial s_4}{\partial u_1} \frac{\partial u_1}{\partial \hat{\varsigma}_9} \frac{\partial \hat{\varsigma}_9}{\partial t} + \frac{\partial V_4}{\partial s_4} \frac{\partial s_4}{\partial u_1} \frac{\partial u_1}{\partial \hat{m}} \frac{\partial \hat{m}}{\partial t}$$
$$+ \frac{\partial V_4}{\partial s_4} \frac{\partial s_4}{\partial u_1} \frac{\partial u_1}{\partial w_4} \frac{\partial w_4}{\partial t} \tag{55}$$

Substitution the adaptation laws of $\dot{w}_4$, $\dot{\hat{\varsigma}}_9$ and $\dot{\hat{m}}$, yields:

$$\frac{dV_4}{dt} = -s_4 \frac{\partial s_4}{\partial u_1} \frac{1}{\cos\chi_1 \cos\chi_3} \alpha_4 \mathrm{sgn} \left(\frac{\partial s_4}{\partial u_1} \right) \chi_8{}^2 \cos\chi_1 \cos\chi_3 s_4{}^\vartheta$$
$$- s_4 \frac{\partial s_4}{\partial u_1} \frac{1}{\cos\chi_1 \cos\chi_3} \beta_4 \mathrm{sgn} \left(\frac{\partial s_4}{\partial u_1} \right) \kappa_4{}^2 \cos\chi_1 \cos\chi_3 s_4$$
$$- s_4 \frac{\partial s_4}{\partial u_1} \frac{1}{\cos\chi_1 \cos\chi_3} \beta_4 \mathrm{sgn} \left(\frac{\partial s_4}{\partial u_1} \right) \xi_4^T \xi_4^T \cos\chi_1 \cos\chi_3 s_4 \tag{56}$$

By simplification and considering $\mathrm{sgn}(\frac{\partial s_4}{\partial u_1}) = \left| \frac{\partial s_4}{\partial u_1} \right| / \frac{\partial s_4}{\partial u_1}$, we have:

$$\frac{dV_4}{dt} = -\alpha_4 \left| \frac{\partial s_4}{\partial u_1} \right| \chi_8{}^2 s_4{}^{\vartheta+1} - \beta_4 \left| \frac{\partial s_4}{\partial u_1} \right| \kappa_4{}^2 s_4{}^2$$
$$- \left| \frac{\partial s_4}{\partial u_1} \right| \xi_4^T \xi_4^T s_4{}^2 \tag{57}$$

Considering $\gamma = \frac{\vartheta+1}{2}$, there are γ_7 and γ_8 such that:

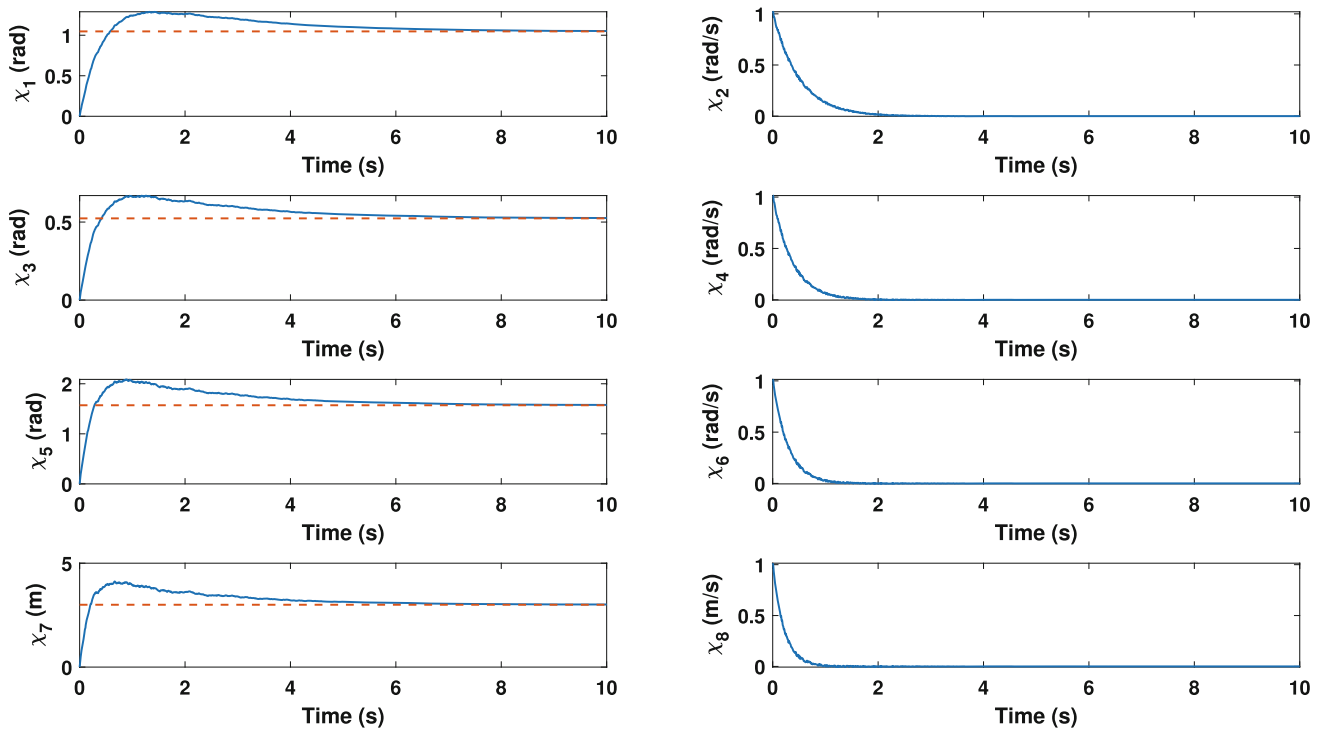$$\dot{V}_4 \leq -\mu_7 V_4{}^\gamma - \mu_8 V_4 \tag{58}$$

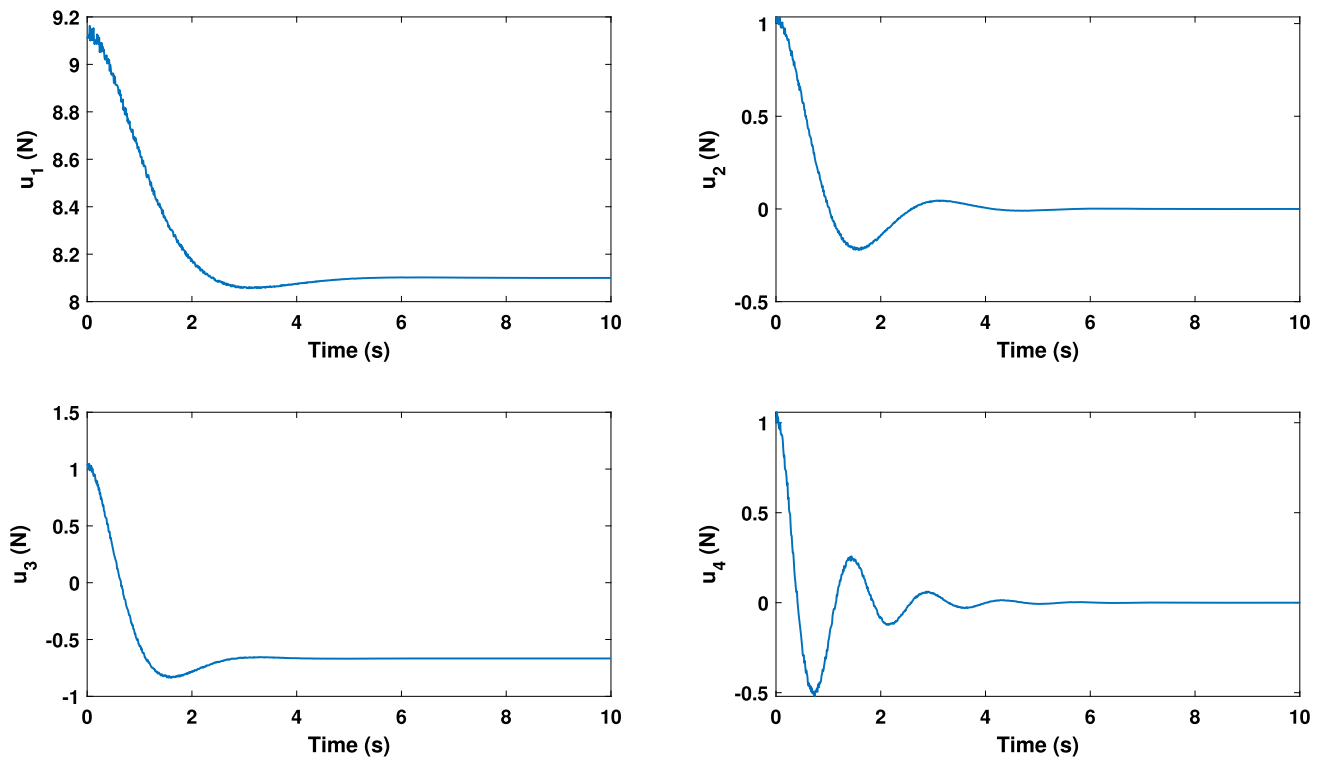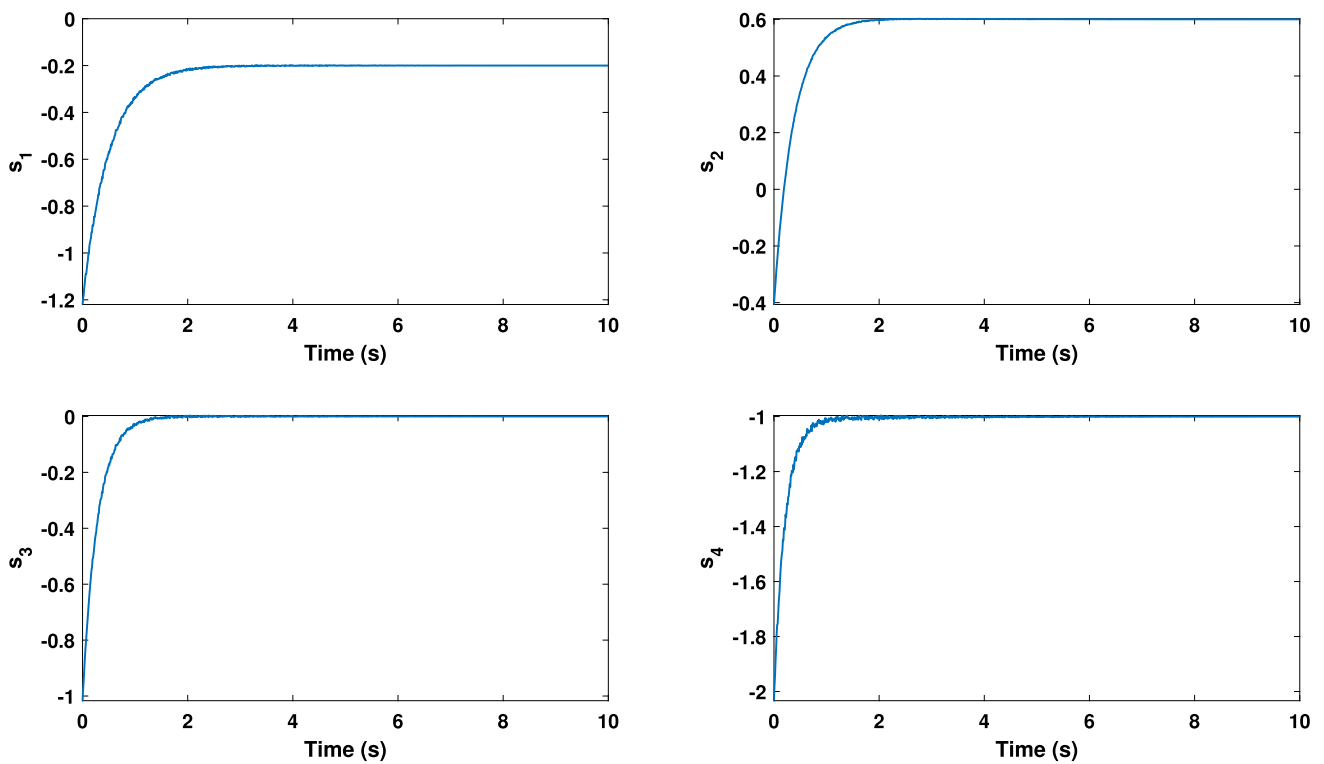**Fig. 5** Output signals

Fig. 6 Control signals

Fig. 7 Sliding surface

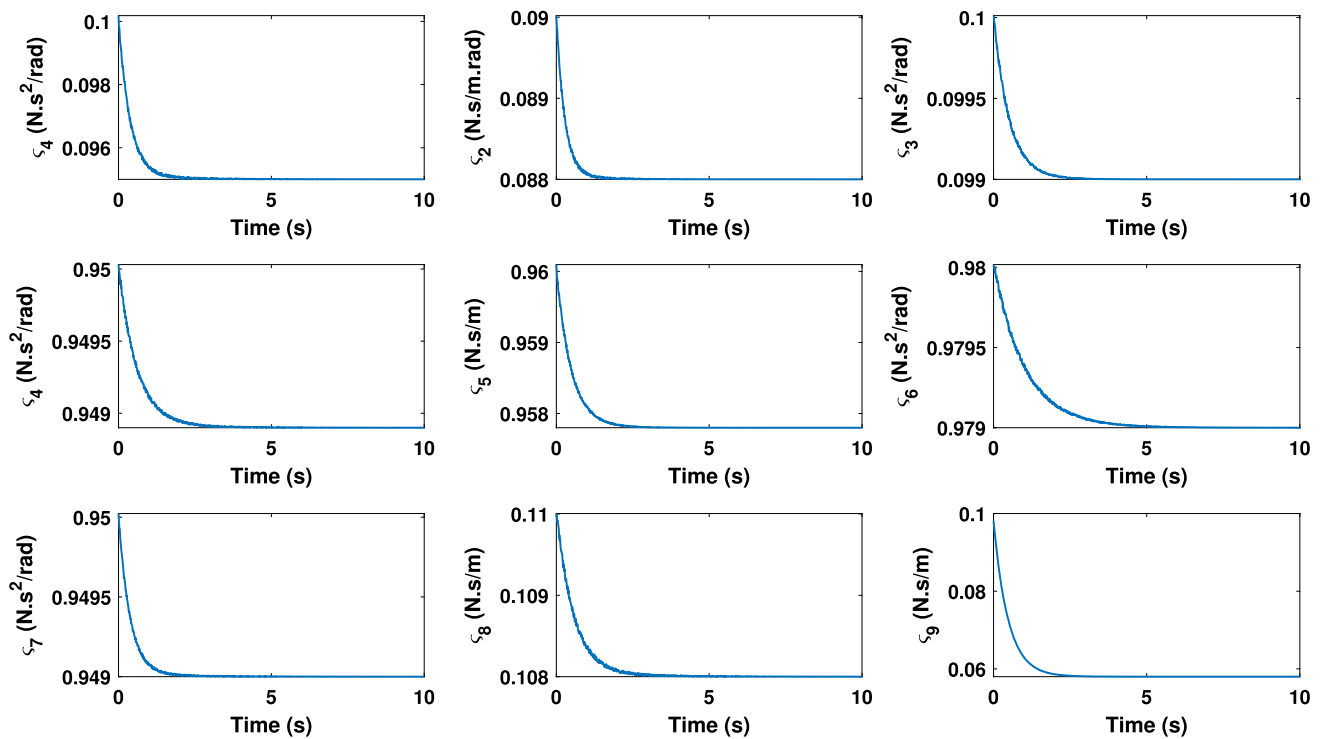**Fig. 8** Adaptation trajectories

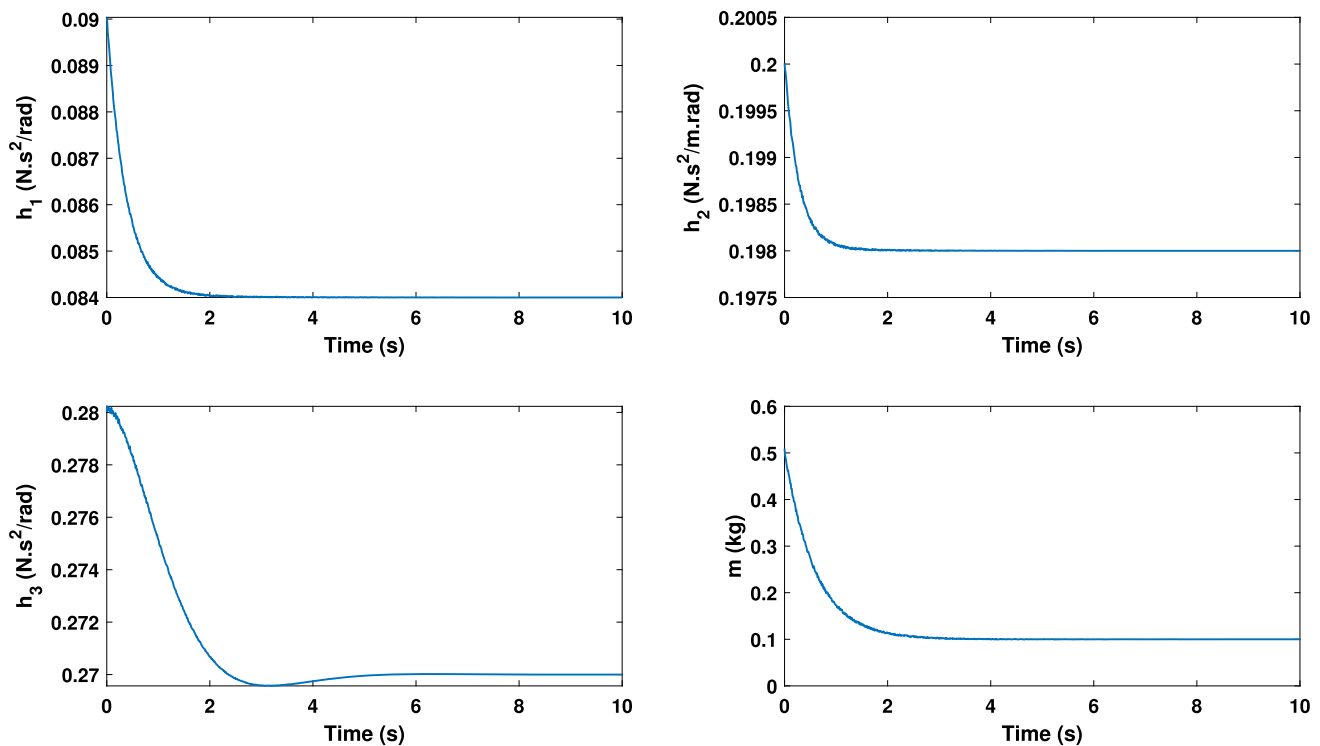**Fig. 9** Adaptation trajectories

where

$$\mu_7 \leq 2^\gamma \alpha_4 \chi_8^2 \left| \frac{\partial s_4}{\partial u_1} \right|$$

$$\mu_8 \leq 2\beta_4 \kappa_4^2 \left| \frac{\partial s_4}{\partial u_1} \right| \tag{59}$$

□

Remark 1 The suggested controller can be developed considering mismatched uncertain disturbances [34], hybrid models [35], and new disturbance rejection methods [36].

Simulation

The initial condition is considered as $\chi_i(0) = 0.10$ ($\forall i = 1, \ldots, 8$). The initial condition of adaptation rules are considered as: $\hat{\varsigma}_i(0) = 0.10$ ($\forall i = 1, \ldots, 9$), $\hat{h}_1(0) = 0.10$, $\hat{h}_2(0) = 0.20$, $\hat{h}_3(0) = 0.30$ and $\hat{m}(0) = 0.65$. The designing parameters are considered as: $\alpha_1' = \alpha_2' = 2$, $\alpha_3' = \alpha_4' = 2$, $k_1 = k_2 = 10$, $k_3 = k_4 = 5$, $\alpha_i = 0.05$ ($\forall i = 1, \ldots, 4$), $\beta_i = 0.05$ ($\forall i = 1, \ldots, 4$), $\vartheta = \frac{3}{7}$. The reference parameters are considered as: $\varphi_d = \frac{\pi}{3}$, $\Theta_d = \frac{\pi}{6}$, $\Omega_d = \frac{\pi}{2}$, and $z_d = 3$. It should be noted that the suggested controller is adaptive, and there is no such big restriction on choosing the control parameters. (Table 1) The trajectories of states are shown in Fig. 5. The results show that

$[\chi_1, \chi_3, \chi_5, \chi_7] = [\varphi, \Theta, \Omega, z]$ follow the reference values $[\varphi_d, \Theta_d, \Omega_d, z_d]$. The stabilization of other states is done in a limited time. The simulations show that by the use of the suggested method, the transient responses are faster and smoother. From (53) the time period is computed as follows. Suppose $t_0 = 0$ and $\gamma = \frac{\vartheta+1}{2} = \frac{3/7+1}{2} = 0.71$. From (48), μ_1 and μ_2 are computed as:

$$\mu_1 \leq 2^\gamma \alpha_1 \left| \frac{\partial s_1}{\partial u_2} \right| \left[(\chi_4 \chi_6)^2 + (\bar{\Phi}\chi_4)^2 + \chi_2^4 \right] = 0.00002425,$$

$$\mu_2 \leq 2\kappa_1^2 \beta_1 \left| \frac{\partial s_1}{\partial u_2} \right| = 30.97 \tag{60}$$

By replacing μ_1 and μ_2 in (53), the time period is computed as $t_{s_1} = 2.6$. The others are computed in same way and we have $t_{s_2} = 2.72$, $t_{s_3} \simeq 4.21$, $t_{s_4} = 5.19$.

The control signals are shown in Fig. 6. The signals are smooth with suitable magnitude and fluctuation. The sliding surface is given in Fig. 7. This figure shows that the sliding surface works well and it converges to zero in a short time. The sliding surface converges to zero faster than conventional methods. The sliding signals demonstrate finite-time convergence. The convergence of free parameters is given in Figs. 8 and 9. We see that unknown parameters are converged in a finite time. The trajectories of adapted parameters are smooth and fast. According to simulations, it can be approved that

Table 2 MSE comparison

Signal	Controller	
	Proposed controller	T2-FLS-based controller [21]
$\chi_1 - \varphi_d$	0.0284	0.1870
χ_2	0.0262	0.5012
$\chi_3 - \Theta_d$	0.0069	0.0781
χ_4	0.0196	0.1305
$\chi_5 - \Omega_d$	0.0612	0.0517
χ_6	0.0153	0.0410
$\chi_7 - z_d$	0.2236	0.2874
χ_8	0.0115	0.2864

the suggested control is effective for time-limited tracking of the UAVs. To better demonstrate the applicability of the suggested controller, the results are compared with a similar T2-FLS-based controller [21]. In [21], a T2-FLS controller is designed for UAVs, and its accuracy is compared with PID. The designed system is tested using a software-in-the-loop simulator and actual flight experiments. The compared mean square errors (MSEs) are given in Table 2. The values of MSE show that the suggested T3-FLS based controller has better results.

Conclusion

In this paper, the adaptation laws for the dynamic model are derived through the stability analysis, and adaptation error is compensated by an adaptive T3-FLS. The suggested T3-FLS is trained to improve the stability and eliminate the effect of adaptation error of parameters and disturbances. The designed scheme is applied to a case-study UAV with unknown dynamics perturbed by disturbances. The core concept involves incorporating the fundamental dynamics of UAVs and devising adaptation laws to improve modeling precision. Additionally, an optimized T3-FLS with SMC is implemented to eradicate adaptation errors and guarantee robustness. The simulations show the efficacy of the proposed method in achieving rapid and smooth transient responses, as well as the stabilization of various states within a constrained timeframe. The sliding surface demonstrates exceptional performance, swiftly converging to zero and surpassing traditional methods. Moreover, the adaptation of unknown parameters exhibits finite-time convergence, characterized by smooth and expeditious trajectories. Ultimately, the simulation outcomes affirm the effectiveness of the developed control approach for time-constrained tracking and stability of UAVs, thereby contributing to advancements in the field of control systems and robotics.

Data availability The paper presents no data.

Declaration

Conflict of interest The authors declare that they have no conflict of interest.

References

1. Azar AT, Sardar MZ, Ahmed S, Hassanien AE, Kamal NA (2023) Autonomous robot navigation and exploration using deep reinforcement learning with gazebo and ros. In: International Conference on Advanced Intelligent Systems and Informatics, Springer, pp 287–299

2. Dong B, Wang Y, Chen J, Zhang Z, An T (2023) Decentralized robust interaction control of modular robot manipulators via harmonic drive compliance model-based human motion intention identification. Complex Intell Syst 9(2):1247–1263

3. Candan F, Dik OF, Kumbasar T, Mahfouf M, Mihaylova L (2023) Real-time interval type-2 fuzzy control of an unmanned aerial vehicle with flexible cable-connected payload. Algorithms 16(6):273

4. Mahmoud TA, El-Hossainy M, Abo-Zalam B, Shalaby R (2024) Fractional-order fuzzy sliding mode control of uncertain nonlinear mimo systems using fractional-order reinforcement learning. Complex Intell Syst pp 1–29

5. Abd-Elhaleem S, Hussien MA, Hamdy M, Mahmoud TA (2023) Event-triggered model-free adaptive control for nonlinear systems using intuitionistic fuzzy neural network: simulation and experimental validation. Complex Intell Syst pp 1–27

6. Dong B, Jing Y, Zhu X, Cui Y, An T (2023) Adaptive impedance decentralized control of modular robot manipulators for physical human-robot interaction. J Intell Robot Syst 109(3):48

7. Wang J, Zhu B, Zheng Z (2023) Robust adaptive control for a quadrotor uav with uncertain aerodynamic parameters. IEEE Trans Aerosp Electron Syst

8. Nekoo SR, Acosta J, Ollero A (2023) Combination of terminal sliding mode and finite-time state-dependent riccati equation: Flapping-wing flying robot control. Proc Inst Mech Eng Part I J Syst Control Eng 237(5):870–887

9. Belmouhoub A, Bouzid Y, Medjmadj S, Derrouaoui SH, Siguerdidjane H, Guiatni M (2023) Fast terminal synergetic control for morphing quadcopter with time-varying parameters. Aerosp Sci Technol 141:108540

10. Mohammadzahri M, Khaleghifar A, Ghodsi M, Soltani P, AlSulti S (2023) A discrete approach to feedback linearization, yaw control of an unmanned helicopter. Unmanned Syst 11(01):57–66

11. Jin Z, Li D, Xiang J (2023) Robot pilot: A new autonomous system toward flying manned aerial vehicles. Engineering

12. Abdelghany MB, Moustafa AM, Moness M (2022) Benchmarking tracking autopilots for quadrotor aerial robotic system using heuristic nonlinear controllers. Drones 6(12):379

13. Abed AM, Rashid ZN, Abedi F, Zeebaree SR, Sahib MA, Mohamad Jawad AJ, Redha Ibraheem GA, Maher RA, Abdulkareem AI, Ibraheem IK et al (2022) Trajectory tracking of differential drive mobile robots using fractional-order proportional-integral-derivative controller design tuned by an enhanced fruit fly optimization. Meas Control 55(3–4):209–226

14. Li Y, Zhu X, Yin G (2023) Robust actuator fault detection for quadrotor uav with guaranteed sensitivity. Control Eng Pract 138:105588

15. Ahmed S, Azar AT (2023) Adaptive fractional tracking control of robotic manipulator using fixed-time method. Complex Intell Syst 10:1–14

16. Can A, Price J, Montazeri A (2022) A nonlinear discrete-time sliding mode controller for autonomous navigation of an aerial vehicle using hector slam. IFAC-PapersOnLine 55(10):2653–2658

17. Baba A, Alothman B (2023) A fuzzy logic-based stabilization system for a flying robot, with an embedded energy harvester and a visual decision-making system. Robot Auton Syst 167:104471

18. Mammadova K, Hamzayev S (2023) Motion trajectory planning of a mobile robot flying in a fuzzy environment. Sci Collect «InterConf+» 33 (155): 375–385

19. Kumar R, Singh UP, Bali A, Chouhan SS (2023) It2-neuro-fuzzy wavelet network with jordan feedback structure for the control of aerial robotic vehicles with external disturbances. In: Deep Learning and Other Soft Computing Techniques: Biomedical and Related Applications, Springer, pp 195–207

20. Ansarian A, Mahmoodabadi M (2023) Multi-objective optimal design of a fuzzy adaptive robust fractional-order pid controller for a nonlinear unmanned flying system. Aerosp Sci Technol 141:108544

21. Hailemichael A, Karimoddini A (2023) Development of a robust interval type-2 tsk fuzzy logic controlled uav platform. J Intell Robot Syst 107(2):27

22. Qadir S, Khatoon S, Shahid M (2023) Comparison of conventional, modern and intelligent control techniques on uav control. In: 2023 International Conference on Power, Instrumentation, Energy and Control (PIECON), IEEE, pp 1–6

23. Pussente GA, de Aguiar EP, Marcato AL, Pinto MF (2023) Uav power line tracking control based on a type-2 fuzzy-pid approach. Robotics 12(2):60

24. Huang H, Xu H, Chen F, Zhang C, Mohammadzadeh A (2023) An applied type-3 fuzzy logic system: practical matlab simulink and m-files for robotic, control, and modeling applications. Symmetry 15(2):475

25. Wu L, Huang H, Wang M, Alattas KA, Mohammadzadeh A, Ghaderpour E (2023) Optimal control of non-holonomic robotic systems based on type-3 fuzzy model. IEEE Access

26. Melin P, Castillo O (2023) An interval type-3 fuzzy-fractal approach for plant monitoring. Axioms 12(8):741

27. Castillo O, Castro JR, Melin P (2023) Forecasting the covid-19 with interval type-3 fuzzy logic and the fractal dimension. Int J Fuzzy Syst 25(1):182–197

28. Mohammadzadeh A, Taghavifar H, Zhang C, Alattas KA, Liu J, Vu MT (2024) A non-linear fractional-order type-3 fuzzy control for enhanced path-tracking performance of autonomous cars. IET Control Theory Appl 18(1):40–54

29. Taghavifar H, Mohammadzadeh A, Zhang W, Zhang C (2023) Non-singleton gaussian type-3 fuzzy system with fractional order ntsmc for path tracking of autonomous cars. ISA Trans

30. Elhaki O, Shojaei K, Mohammadzadeh A (2023) Robust state and output feedback prescribed performance interval type-3 fuzzy reinforcement learning controller for an unmanned aerial vehicle with actuator saturation. IET Control Theory Appl 17(5):605–627

31. Singh DJ, Verma NK (2024) Interval type-3 ts fuzzy system for nonlinear aerodynamic modeling. Appl Soft Comput 150:111097

32. Bouadi H, Bouchoucha M, Tadjine M (2007) Modelling and stabilizing control laws design based on backstepping for an uav type-quadrotor. IFAC Proc Vol 40(15):245–250

33. Bouadi H, Bouchoucha M, Tadjine M (2007) Sliding mode control based on backstepping approach for an uav type-quadrotor. World Acad Sci Eng Technol 26(5):22–27

34. Yang G (2023) Asymptotic tracking with novel integral robust schemes for mismatched uncertain nonlinear systems. Int J Robust Nonlinear Control 33(3):1988–2002

35. Emadi A, Ozen M, Abdi A (2022) A hybrid model to study how late long-term potentiation is affected by faulty molecules in an intra-neuronal signaling network regulating transcription factor CREB. Integr Biol 14(5):111–125

36. Yang G, Yao J (2024) Multilayer neurocontrol of high-order uncertain nonlinear systems with active disturbance rejection. Int J Robust Nonlinear Control 34(4):2972–2987